6-12-2007

Numerical Modeling of a Gravity Wave Packet Ducted by the Thermal Structure of the Atmosphere

Yonghui Yu
Embry-Riddle Aeronautical University

Michael P. Hickey Ph.D.
Embry-Riddle Aeronautical University, hicke0b5@erau.edu

Scholarly Commons Citation

Yu, Y., and M. P. Hickey (2007), Numerical modeling of a gravity wave packet ducted by the thermal structure of the atmosphere, J. Geophys. Res., 112, A06308, doi: https://doi.org/10.1029/2006JA012092

Numerical modeling of a gravity wave packet ducted by the thermal structure of the atmosphere

Yonghui Yu[1,2] and Michael P. Hickey[1,2]

Received 18 September 2006; revised 2 December 2006; accepted 7 February 2007; published 12 June 2007.

[1] A time-dependent and fully nonlinear numerical model is employed to solve the Navier-Stokes equations in two spatial dimensions and to describe the propagation of a Gaussian gravity wave packet generated in the troposphere. A Fourier spectral analysis is used to analyze the frequency power spectra of the wave packet, which propagates through and dwells within several thermal ducting regions. The frequency power spectra of the wave packet are derived at several discrete altitudes, which allow us to determine the evolution of the packet. This spectral analysis also clearly reveals the existence of a stratospheric duct, a mesospheric and lower thermospheric duct, and a duct lying between the tropopause and the lower thermosphere. In addition, we determine the spatially localized wave kinetic energy density and the horizontally averaged, time-resolved, normalized vertical velocity. Examination of these diagnostic variables allows us to better understand the process of wave ducting and the vertical transport of wave energy among multiple thermal ducts. The spectral analysis allows us to unambiguously identify the ducted wave modes. These results compare favorably with those derived from a full-wave model.

Citation: Yu, Y., and M. P. Hickey (2007), Numerical modeling of a gravity wave packet ducted by the thermal structure of the atmosphere, *J. Geophys. Res.*, *112*, A06308, doi:10.1029/2006JA012092.

1. Introduction

[2] Theoretical and numerical studies have shown that atmospheric gravity waves (AGWs) can be ducted or trapped by the vertical variations of atmospheric temperature and winds [*Pitteway and Hines*, 1965; *Friedman*, 1966; *Wang and Tuan*, 1988; *Fritts and Yuan*, 1989; *Hecht et al.*, 2001; *Hickey*, 2001; *Walterscheid et al.*, 2001; *Snively and Pasko*, 2003, 2005; *Yu and Hickey*, 2007; Y. Yu and M.P. Hickey, Simulated ducting of high-frequency atmospheric gravity waves in the presence of background winds, submitted to *Geophys. Res. Lett.*, hereinafter referred to as Yu and Hickey, submitted manuscript, 2007a]. A large number of observations have also provided a better understanding of the ducting processes [*Hines and Tarasick*, 1994; *Taylor et al.*, 1995a, 1995b; *Isler et al.*, 1997; *Hecht et al.*, 1997; *Walterscheid et al.*, 1999]. The airglow imager measurements of *Walterscheid et al.* [1999] were interpreted as being due to quasi-monochromatic (QM) waves that were ducted or trapped in the lower thermospheric thermal duct or between the ground and the evanescent layer above the duct. Subsequently, *Hecht et al.* [2001] observed periodic coherent wave structures propagating horizontally across the field of view of their airglow images ($\sim$200 km) and reasoned that they were QM waves. The observed QM waves typically had horizontal phase speeds less than 100 m/s, horizontal wavelengths on an order of tens of kilometers, and periods of several minutes.

[3] In the absence of ducting, only freely propagating gravity waves would be observable as they propagate obliquely upward through airglow regions. In this case, the waves could be observed in a fairly close proximity ($\sim$100–200 km horizontally) to their source region in the troposphere. *Walterscheid et al.* [1999] argued that the QM waves seen in the airglow images over Adelaide, Australia (35°S, 138°E) might be ducted or trapped because there were no local sources that would have generated freely propagating waves. It was suggested that the wave source was most probably remote (several thousand kilometers away) and located over the northern Australian coast where intense convective activity often occurs. The possibility for such an explanation was explored using a full-wave model [*Hickey*, 1988a, 1988b; *Hickey et al.*, 1997, 1998] that confirmed the existence of a lower thermospheric thermal duct lying between the mesopause and an altitude of about 140 km. Moreover, the ducting was believed to be quite different from the Doppler ducts discussed by *Isler et al.* [1997].

[4] In the past, several modeling studies of gravity wave ducting have been presented by different authors. For example, *Fritts and Yuan* [1989] provided solutions to the one-dimensional Taylor-Goldstein equation to study waves ducted in thermal and Doppler ducts. *Walterscheid et al.* [2001] simulated the propagation of waves from a tropical convective storm and their subsequent ducting in a thermal duct using a two-dimensional cylindrical coordinate system.

[1]Department of Physical Sciences, Embry-Riddle Aeronautical University, Daytona Beach, Florida, USA.
[2]Department of Physics, University of Central Florida, Orlando, Florida, USA.

0148-0227/07/2006JA012092

Most recently, *Snively* [2003] used Gaussian wave packets in a two-dimensional model to simulate nonlinear wave breaking in the far-field lower thermospheric thermal duct. Inspired by these previous studies, we perform simulations using a time-dependent, nonlinear two-dimensional model (which we have called atmospheric gravity waves for the Earth plus tides and planetary waves [AGE-TIP] and will describe later) to better understand the ducting processes. To this end, we specifically analyze the spatially localized wave kinetic energy density and the horizontally averaged, time-resolved, normalized vertical velocity. In addition, we perform a spectral analysis at various discrete altitudes to help identify those waves in the packet that are selectively ducted. In so doing, we will learn more about the QM waves discussed by *Walterscheid et al.* [1999]. The AGE-TIP model clearly demonstrates the duct characteristics that include the evolution of the ducting, the coupling between ducts, and their persistence. The model is configured in a horizontally infinite domain to facilitate comparisons with a full-wave model [*Hickey*, 2001] and with the full-wave model results presented by *Hecht et al.* [2001].

[5] Mean winds affect wave ducting by altering the intrinsic wave period (and therefore the vertical wave number) and causing it to vary with height in the real atmosphere. Here we have chosen to deliberately exclude the effects of mean winds so that we can focus on the thermal ducting process alone. The neglect of mean winds also allows us to determine unambiguous frequency spectra at various heights. In a windless atmosphere, the altitude variation of the Brunt-Väisälä frequency is responsible for the wave thermal ducting. *Hines* [1960] formulated a dispersion relation that can be solved for the square of the vertical wave number (m^2) as

$$m^2 = \frac{(N^2 - \omega^2)}{\omega^2} k^2 + \frac{(\omega^2 - \omega_a^2)}{C^2}, \tag{1}$$

where ω is the extrinsic frequency observed on the ground, C is the sound speed, N is the Brunt-Väisälä frequency, ω_a is the acoustic cutoff frequency, and k is the horizontal wave number. An atmospheric gravity wave thermal duct could exist when two evanescent regions ($m^2 < 0$) sandwich an internal region ($m^2 > 0$), which from equation (1) implies that the thermal duct is located in the vicinity of a region of a local maximum of N. Ducting also requires that a standing wave fits within the internal region ($m^2 > 0$) between the duct upper and lower boundaries with a half-integer number of local vertical wavelengths. Another condition required for strong ducting is that the evanescent regions below and above the duct are thick enough to efficiently reflect the ducted waves. Therefore only certain combinations of wave period and horizontal wavelength favor strong ducting in atmospheric thermal ducts.

[6] Although equation (1) is based essentially on the linear gravity wave theory, according to *Zhang et al.* [2000], it can still be feasible in the nonlinear circumstance they considered. *Fritts* [1984] provided a measure of the importance of nonlinearity by considering the ratio of the horizontal perturbation velocity (u') to the horizontal phase speed (c) of the wave. Waves for which $|u'| \ll c$ are linear, while waves for which $|u'| \sim c$ are nonlinear. Since most ducted waves are shorter period waves, much of the wave energy resides in high-frequency, fast wave modes, and so, if the wave amplitude is kept relatively small, the nonlinearity should not be an issue. Slower wave modes would be viscously damped at higher altitudes in the thermosphere. Our AGE-TIP model is a nonlinear model, and so it accounts for such effects without ever using a dispersion relation. In the present study, we use the dispersion relation only to estimate altitudes of evanescence most of which lie below the thermosphere.

[7] The layout of this paper is as follows. The model equations are introduced in section 2. The spectral analysis, wave kinetic energy density, and normalized vertical velocity are presented and described in detail in section 3. Discussion and conclusion are presented in sections 4 and 5, respectively.

2. Model

[8] The model is acronymically named atmospheric gravity waves for the Earth plus tides and planetary waves (AGE-TIP). The equations solved in the AGE-TIP model are the Navier-Stokes equations, which involve the mass continuity, momentum, and thermodynamic energy equations, plus the definition of potential temperature and the equation of state for an ideal gas. These highly coupled equations include dissipation due to eddy processes and molecular processes (viscosity and thermal conduction). The initial atmosphere is nonisothermal, and here horizontal mean winds are neglected. Our reason for neglecting the mean winds is based on our desire to study the thermal ducting alone, thereby providing a control experiment for future studies that include mean winds. Our analysis of wave ducting in the presence of background winds can be found in the works of Yu and Hickey [submitted manuscript, 2007a; Y. Yu and M. P. Hickey, Nonlinear secondary generation of multiple gravity wave packets in the lower thermosphere region of wind shear, submitted to *Journal of Geophysical Research*, hereinafter referred to as Yu and Hickey, submitted manuscript, 2007b]. The Coriolis force (owing to the rotation of the Earth) and ion drag are also neglected [Y. Yu and M.P. Hickey, A numerical model characterizing internal gravity wave propagation into the upper atmosphere, submitted to *Journal of Geophysical Research*, hereinafter referred to as Yu and Hickey, submitted manuscript, 2007c]. The Coriolis force and ion drag are both negligible for high-frequency gravity waves (see the Discussion section). Composition effects in the thermosphere associated with an altitude variation of the mean molecular weight [*Walterscheid and Hickey*, 2001] are also neglected because our primary region of interest is the atmospheric region below the thermosphere. This is discussed in more detail in the Discussion section.

$$\frac{D\rho}{Dt} + \rho \underline{\nabla} \cdot \underline{v} = 0, \tag{2}$$

$$\rho \frac{D\underline{v}}{Dt} + \underline{\nabla} p - \rho \underline{g} - \underline{\nabla} \cdot (\rho \upsilon \underline{\nabla} \mathrm{v}) - \underline{\nabla} \cdot (\rho \eta_e \underline{\nabla} \mathrm{v}) + \rho K_R \underline{v} = 0, \tag{3}$$

$$\rho c_v \frac{DT}{Dt} + p \underline{\nabla} \cdot \underline{v} - \underline{\nabla} \cdot (\lambda_m \underline{\nabla} T) - \frac{c_v \overline{T}}{\overline{\theta}} \underline{\nabla} \cdot (\rho \kappa_e \underline{\nabla} \theta) + c_v \rho K_N T = \rho c_v (Q_i + Q_w), \tag{4}$$

$$\theta = T\left(\frac{\overline{p}_{00}}{p}\right)^{\kappa}, \tag{5}$$

$$p = \frac{\rho R^* T}{M}. \tag{6}$$

[9] The model domain is in two spatial dimensions, where x is the horizontal coordinate, z is the vertical coordinate, and t is time. The model extends vertically from the ground up to 250-km altitude, and it horizontally spans one horizontal wavelength allowing periodic boundary conditions to be imposed. These nonlinear equations are used to describe fully compressible, nonhydrostatic plane wave motions. v is the normal velocity vector with x (positive eastward) and z (positive upward) components u and w, respectively; ρ is the atmospheric neutral density; p is the atmospheric pressure; g is the acceleration due to gravity; υ is the molecular viscosity; η_e is the eddy momentum diffusivity; c_v and c_p are the specific heats at constant volume and constant pressure, respectively; Q_i is the atmospheric heat source initially introduced to balance the thermodynamic energy equation; Q_w is the wave thermal excitation; T is the atmospheric temperature; λ_m is the molecular thermal conductivity; κ_e is the eddy thermal diffusivity; M is the mean molecular weight; and K_R and K_N are Rayleigh friction and Newtonian cooling coefficients, respectively. The operator $D/Dt = \partial/\partial t + \underline{v}\cdot\nabla$ is the substantial derivative, where $\underline{v}$ (x, z, t) is the total velocity vector (mean plus perturbation). θ is the potential temperature, $\overline{p}_{00}$ = 1000 mbar (the over-bar represents a horizontally averaged value) is the reference pressure on the ground, $\kappa = R/c_p$, $R = R^*/M$, and R^* is the universal gas constant. The governing equations (2)–(6) in the AGE-TIP model have been used for one-dimensional, linear steady state in previous applications in *Hickey et al.* [2000, 2003], *Hickey* [2001] and *Hickey and Yu* [2005].

[10] A time-splitting technique is used to integrate the finite difference equations derived from the model equations. Using an explicit second-order Lax-Wendroff scheme, the first-half integration is implemented in the convective part of the equations. The second-half integration is performed iteratively in the remainder of the equations using an implicit Newton-Raphson scheme. The vertical momentum equation and the thermodynamic energy equation use both schemes, but the mass continuity equation and the horizontal momentum equation use the second-order Lax-Wendroff scheme only. The primary wave variables are evaluated using a staggered-grid technique similar to that demonstrated by *Taylor* [1984], by which density and pressure (or temperature) are carried at the center of a computational unit box, while the horizontal and vertical mass flux terms, ρu and ρw, are computed at the midpoints of the lateral and top-bottom boundaries of a computational unit box, respectively. The application described above is similar to that of *Walterscheid and Schubert* [1990].

[11] The nominal eddy diffusion coefficients are based on a profile due to *Strobel* [1989] and have large values in the mesopause region. The eddy momentum diffusivity maximizes with a value of 100 $m^2\ s^{-1}$ at 90-km altitude, and the Prandtl number is 3. This maximum value for the eddy diffusivity is comparable to values derived from radar observations of *Hocking* [1987]. A small value of eddy diffusivity (0.1 $m^2\ s^{-1}$) is used for the lower atmosphere. Molecular diffusion coefficients are taken from *Rees* [1989]. Rayleigh friction and Newtonian cooling provide artificial sponge layers near the upper boundary to simulate the radiation conditions. They have large effects near the upper boundary and exponentially decrease with lower altitudes away from the upper boundary. Relevant parameters can be found in *Walterscheid and Schubert* [1990] and also in *Hickey et al.* [2000] and *Hickey and Yu* [2005]. The horizontal and vertical grid spacings are 0.5 km and 1.0 km, respectively. The time step used is 0.7 s. Detailed information about the AGE-TIP model is provided by Yu and Hickey [submitted manuscript, 2007c].

3. Results

[12] In Figure 1, we plot the Brunt-Väisälä frequency as a function of altitude. Also shown is the square of the vertical wave number, m^2, calculated for the primary period of 6.276 min and the horizontal wavelength of 35 km. The atmospheric mean temperature and neutral density are defined by the MSIS-E-90 model [*Hedin*, 1991] for a date of 1993 January 15, a local time of 2200 hours, and a latitude and longitude of 18.5°N and 0.0°, respectively. The Brunt-Väisälä frequency N can be derived, and it is defined by *Fritts* [1984] as

$$N^2(z) = \frac{g}{\overline{T}}\left(\frac{\partial \overline{T}}{\partial z} + \frac{g}{c_p}\right). \tag{7}$$

[13] A previous simulation using the full-wave model [*Hecht et al.*, 2001] to describe a wave generated in the lower troposphere has been used as a basis for the numerical experiments performed here. A wave thermal excitation is chosen explicitly to have a primary period of 6.276 min and a horizontal wavelength of 35 km. The results from the full-wave model indicate that there is a strong lower thermospheric thermal duct existing with this chosen wave mode. There are four wave ducting regions shown in Figure 1, depicting the stratospheric duct (period 5.07 min), the mesospheric duct (period 6.20 min), the lower thermospheric duct (also a period of 6.20 min), and the vertically extended duct (period 7.06 min). According to the m^2 plot derived from equation (1), the stratospheric duct is estimated to lie between altitudes of about 15 and 40 km, the mesospheric duct lies between altitudes of about 50 and 90 km, the lower thermospheric duct lies between altitudes of about 90 and 140 km, and the vertically extended duct lies between altitudes of about 12 and 150 km. These will be discussed in more detail later.

[14] Based on our previous experiences of wave ducting in the lower thermospheric thermal duct [*Walterscheid et al.*, 1999; *Hecht et al.*, 2001], we use the full-wave model to identify those wave parameters that will most likely lead to strong wave trapping in the thermal ducts of the mesosphere and lower thermosphere. Therefore the AGE-TIP model shares the same wave source and geophysical parameters as those used in the full-wave model (location, local time, atmospheric thermal structure, etc.). This also helps facilitate a comparison between the simulations of the two models. The wave thermal excitation varies sinusoidally and periodically over a horizontal wavelength, and periodic boundary conditions at the lateral boundaries imply an

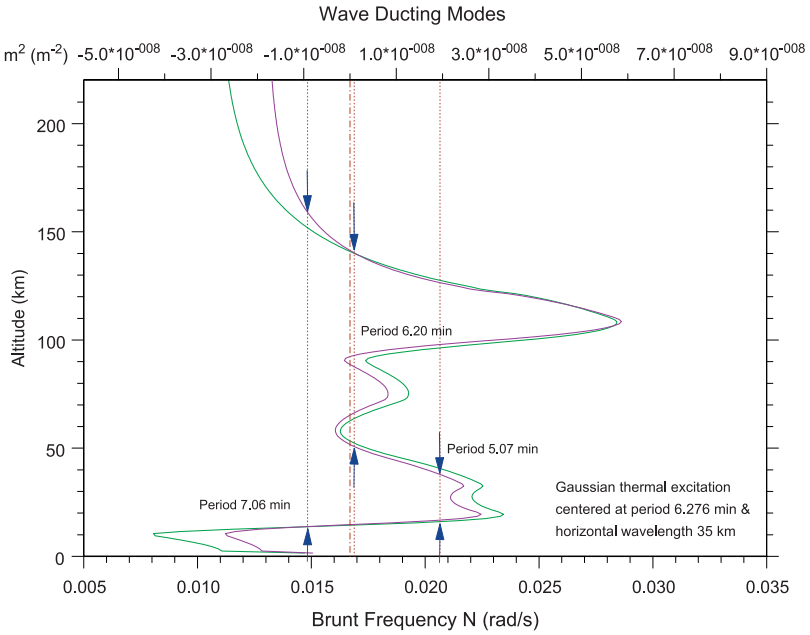

Figure 1. The Brunt frequency N (units in rad s^{-1}, green line, lower x-axis) and the m^2 profile (units in m^{-2}, magenta line, upper x-axis) of the primary wave (period 6.276 min, λ_h = 35 km). The three vertical lines (red, dot-dot) identify waves of period 7.06, 6.20, and 5.07 min. Three pairs of blue arrows identify three individual ducts. The vertical line (red, dash-dot) signifies m = 0 at a period of 6.276 min.

infinite wave train in the horizontal direction. The prescribed source is a Gaussian envelop over altitude of half-width Δz = 0.8 km, centered at altitude ξ = 8 km, and a Gaussian envelop over time of half-width Δt = 6.276 min, centered at time τ = 37.656 min, and with an amplitude of 10^{-5} Ks^{-1}. It is described analytically as

$$Q_w(x,z,t) = 10^{-5}\exp\left(-(t-\tau)^2/2\Delta t^2\right)\exp\left(-(z-\xi)^2/2\Delta z^2\right) \times \sin(k_0 x - \omega_0 t), \quad (8)$$

where $\omega_0 = 2\pi/6.276$ min and $k_0 = 2\pi/35$ km.

[15] The thermal excitation at a fixed position of x = 17.25 km and z = 8 km is plotted as a function of time in Figure 2. In the same figure, we also plot the vertical velocity at the same position as a function of time. From the figure, we see that the vertical velocity and thermal excitation both have a period close to the primary forcing period of 6.276 min and are centered at about 39.08 min. They share an amplitude envelop with time and have an inphase variation. The phase of the vertical velocity accords with the phase of the thermal excitation (keeping pace with

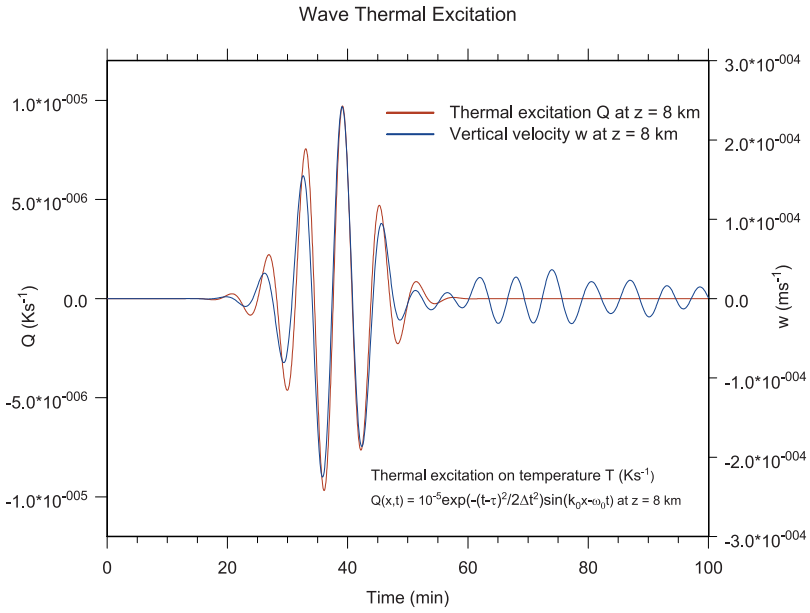

Figure 2. Wave thermal excitation and its resulting vertical velocity at a fixed position of x = 17.25 km and z = 8 km.

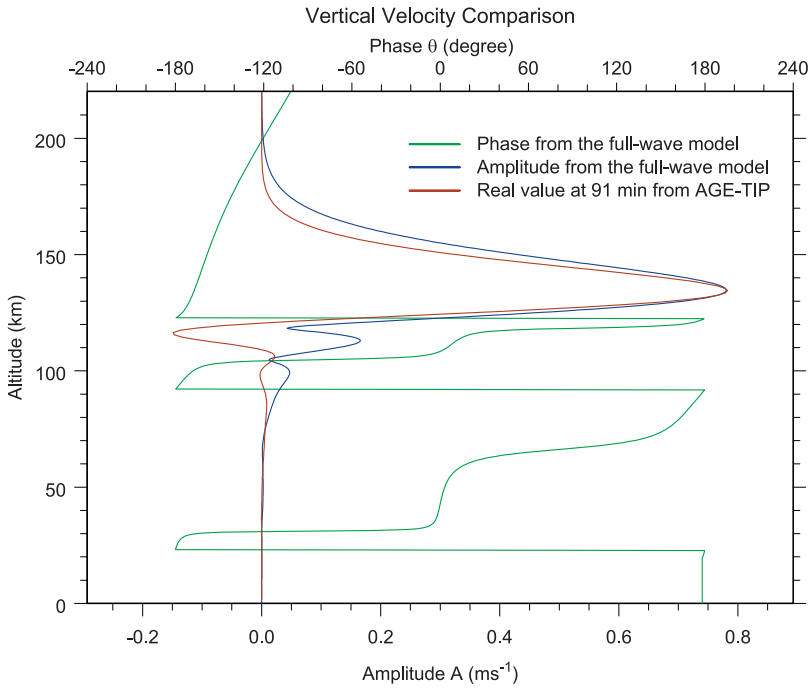

Figure 3. An overall comparison of the vertical velocities between the full-wave (one-dimensional steady state) and AGE-TIP (two-dimensional time-resolved) models.

each other). After the first hour of the simulation, there is still a residual vertical velocity oscillation at altitude 8 km.

[16] In Figure 3, we compare the vertical velocity (w') derived from the AGE-TIP model with that derived from the full-wave model. Because the full-wave model is a steady state model, we show the amplitude and phase of w'. There is a general agreement between the two model simulations. A slight difference between the two sets of model results occurs in the thermosphere. This is largely due to the time dependence of the wave packet simulated in the AGE-TIP model. The wave packet never reaches a steady state, and many frequency components exist at most altitudes. In contrast to this, the full-wave model solutions are steady-state solutions with only one wave frequency present. The overall agreement between the two models suggests that the AGE-TIP model is realistically simulating the propagation of a wave packet from the lower to the upper atmosphere. A more complete comparison between the two sets of model results is given elsewhere (Yu and Hickey, submitted manuscript, 2007c).

[17] In Figure 4, we plot the vertical velocity as a function of time at three discrete altitudes of 110, 130, and 150 km, respectively. At all altitudes considered, residual oscillations are evident after the main wave packet has propagated through those regions. For times between 150 and 350 min, harmonic oscillations are seen at discrete altitudes of 110, 130, and 150 km. These harmonic oscillations are now spectrally analyzed to determine if they are ducted waves.

[18] A Fourier analysis is performed that is inspired by that used by *Alexander* [1996], but here it is in one dimension only and applies to the wave frequency ω. We apply a step function in the other dimension for the horizontal wave number k (λ_h = 35 km). The normalized power spectral density (units in fractions of total power spectrum present at each altitude considered), which results from a Discrete Fourier Transform (DFT) of time series of the vertical velocity, is shown in Figures 5 and 6 for the altitudes of 8, 30, 80, 100, 110, 130, and 150 km. The normalized power spectral density for the wave forcing is also shown. The spectra are calculated using 5-second samples and over the 6 hours of the simulation. The three large peaks seen in the spectra at periods of 7.06 min, 6.20 min, and 5.07 min are identified as wave ducting modes. All three frequencies are seen to exist at 30-km altitude (Figure 5). The 5.07-min spectral peak has an amplitude of about 25.7%, the 7.06-min spectral peak has an amplitude of about 17.7%, and the 6.20-min spectral peak has an amplitude of about 4.4%. The same spectral analysis is also applied to the vertical velocities at altitudes of 20 km and 40 km, and it results in similar spectra (not shown) to that shown for the altitude of 30 km. These three wave modes exist clearly at altitudes of 20, 30, and 40 km. These results imply that the wave with a period of 5.07 min is ducted in the stratospheric duct, and another wave with a period of 7.06 min is ducted between the lower thermosphere and the tropopause. Because of its much lower relative spectral power (only 4.4%) compared to the other two waves (25.7% and 17.7%), we believe that the wave with a period of 6.20 min is not trapped in the stratosphere and is instead freely propagating through this region of the atmosphere. A more detailed analysis of the 6.20-min wave with respect to the stratospheric ducting is provided in the Discussion section. A schematic diagram elucidating the wave ducting modes is shown in Figure 1.

[19] The ducting mode with a period of 6.20 min is seen to be trapped in the mesosphere and lower thermosphere (MLT) region. It clearly resides at altitudes of 80, 110, and 130 km (shown in Figures 5 and 6) and has normalized

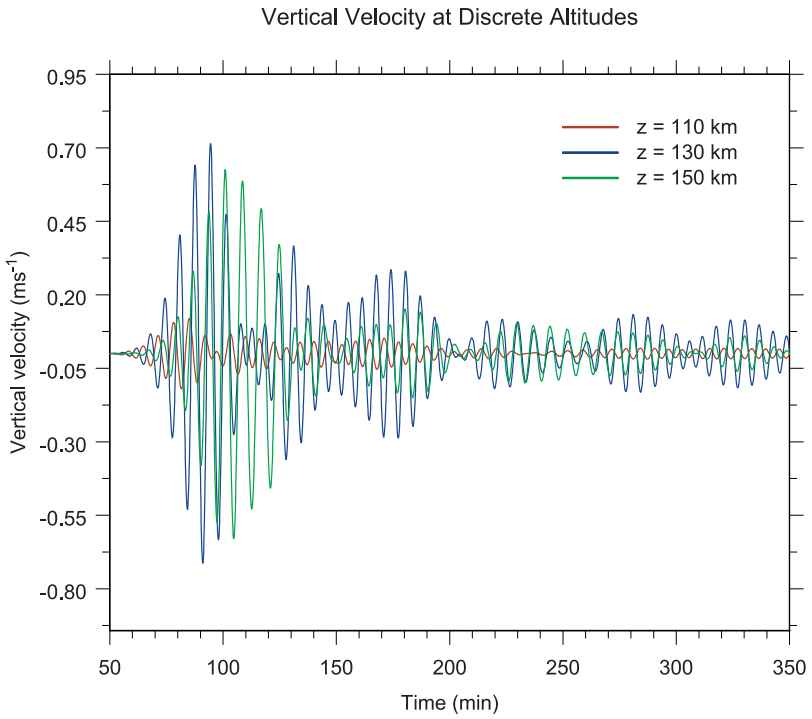

Figure 4. The vertical velocities at discrete altitudes of 110, 130, and 150 km.

spectral amplitudes at each of these altitudes of approximate 37.4%, 29.1%, and 21.1%, respectively. A similar spectral analysis that is applied to the vertical velocities at altitudes of 60, 70, 90, 120, and 140 km results in similar spectra (not shown) to those described above. The ducting mode with a period of 5.07 min is not evident at altitudes of 60 km and above. The fact that, of all the altitudes considered, the 5.07 min wave is evident (through the spectral analysis) only at altitudes of 20, 30, and 40 km supports our belief that this wave is efficiently trapped and ducted in the stratosphere. The ducting mode with a period of 7.06 min appears at all altitudes considered, although some of them are clearly distinguishable (such as the one at 30-km altitude), while others are weak and dominated by other wave modes. The plausibility that this ducting mode resides in the duct between the lower thermosphere and the tropopause is supported by the interpretation of Figure 1.

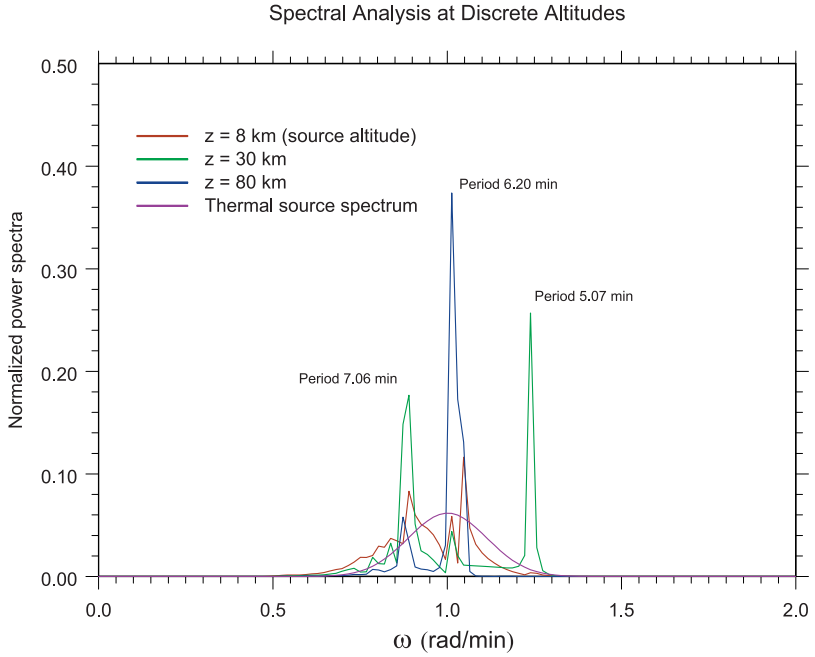

Figure 5. Spectral analysis at discrete altitudes of 8, 30, and 80 km.

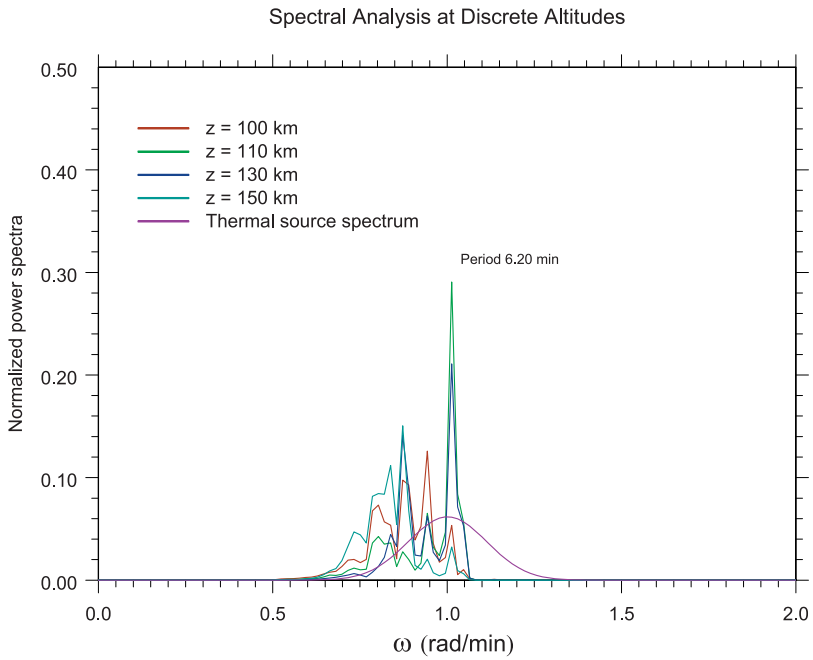

Figure 6. Spectral analysis at discrete altitudes of 100, 110, 130, and 150 km.

[20] Although the 6.20-min mode appears at all altitudes considered, its normalized spectral amplitude has prominent peaks only in two discrete altitude regions. One of these is a thin region centered near 75-km altitude, while the other is a broader region lying between about 90- and 140-km altitude. Inspection of Figure 1 shows that these regions correspond to the regions of a local maximum in the Brunt-Väisälä frequency N. Therefore this mode appears to be ducted in two discrete ducts, one in the mesosphere and the other in the lower thermosphere. They are separated by a thin region near 90-km altitude that corresponds to a local minimum in N. The refractive index, m^2, becomes negative for this wave in a thin region centered near 90-km altitude. The ducting scene is now further examined by considering other diagnostic variables such as the wave kinetic energy density and the normalized vertical velocity. The vertical energy flux is another diagnostic variable discussed elsewhere [*Yu and Hickey*, 2007].

[21] The square root of the wave kinetic energy density, $(u\prime^2 + w\prime^2)\rho/2$ of the packet is shown across the spatial grid at times of about 94 min and about 191 min in Figures 7 and 8, respectively. It exhibits two maxima within a horizontal wavelength as expected for a second-order quantity. By 94 min (Figure 7), the packet has reached the lower thermosphere. The wave energy appears to be concentrated in two separate regions near altitudes of 70 and 130 km. A smaller amount of wave energy is seen near 20-km altitude. After about 3 hours (Figure 8), the wave energy is seen to be concentrated in two separate regions near 25- and 75-km altitude. A smaller amount of wave energy resides near 130-km altitude in the lower thermosphere. Note that the scaling in Figures 7 and 8 is not identical.

[22] The horizontally averaged wave vertical velocity normalized by the square root of the ratio of the densities $((\rho/\rho_{00})^{1/2}w\prime)$, similar to the one used by *Snively and Pasko* [2003], is shown as a function of altitude and time for the 3rd hour of the simulation in Figure 9. Here ρ is the atmospheric neutral density at altitude z, and ρ_{00} is the atmospheric neutral density on the ground ($z = 0$). The packet is restricted to altitudes below about 150 km, and standing waves can be clearly identified between altitudes of about 100 and 120 km and for times between about 120 and 180 min. Standing waves are also evident at this time at altitudes between about 20 and 40 km. In Figure 10, we show the horizontally averaged wave vertical velocity normalized by the square root of the ratio of the densities $((\rho/\rho_{00})^{1/2}w\prime)$ as a function of altitude and time for the 5th hour of the simulation. Standing waves are concentrated in two different regions centered near altitudes of 30 and 110 km. Note that the scaling in Figures 9 and 10 is not identical.

4. Discussion

[23] As a consequence of the periodic boundary conditions imposed at the lateral boundaries, our model domain is essentially of infinite extent in the horizontal direction. Also, the range of possible horizontal wave numbers is restricted because we only prescribe one horizontal wavelength of 35 km in our horizontal periodic domain. To some extent, this restricts our analysis of the horizontal range of the ducted waves because the model precludes direct observation of the horizontal group velocity. However, some estimates of the horizontal range can be made by considering the horizontal group velocity of the waves based on the isothermal dispersion equation. A calculation of the horizontal group velocity from $d\omega/dk$ gives a most realistic value of about 23.5 m/s at 75-km altitude, suggesting that there would be long-range propagation ($\sim$500 km over 6 hours). The observations of *Hecht et al.* [2001] support our expectation of long-range propagation for the ducted waves.

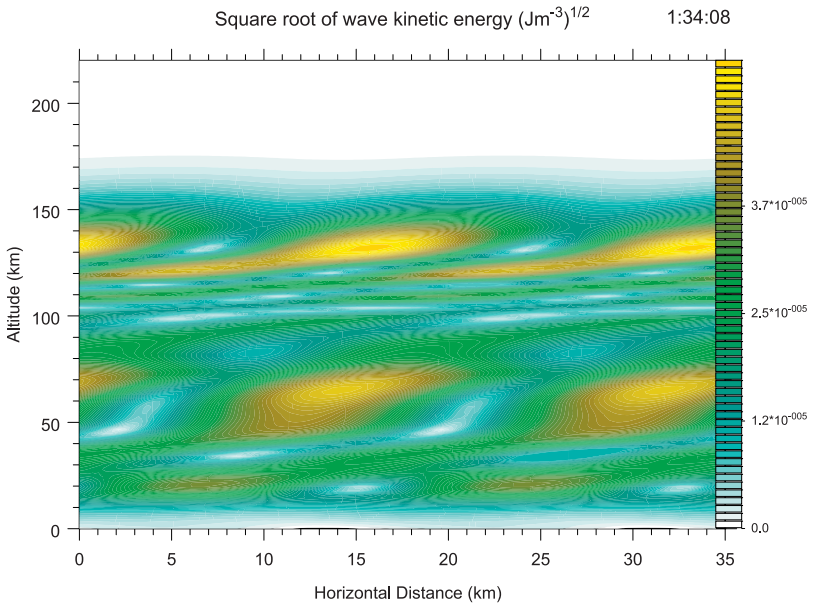

Figure 7. The square root of the wave kinetic energy density, $(u'^2 + w'^2)\rho/2$ of the packet is shown across the spatial grid at a time of about 94 min.

[24] Here we provide some discussion on the reason why the 6.2-min wave is imperfectly ducted in the stratospheric duct. According to the results of the spectral analysis described in the Results section, at stratospheric altitudes, the 6.2-min wave was far weaker than the 5.07-min wave. We attribute this difference to the different vertical structures of the two waves. In particular, for the 6.2-min wave, we find that an integer number of half vertical wavelengths do not fit into the stratospheric duct, whereas the converse is true for the 5.07-min wave. We can provide a rough estimate of the vertical wavelength λ_z for the 6.2-min wave by calculating m^2 at about 27.5-km altitude (close to the midpoint of the stratospheric duct, as shown in Figure 1), where a local minimum of m^2 occurs. We obtain a value for m^2 of about 2.17×10^{-8} (units in m^{-2}), which results in a value of λ_z = 42.65 km, and a half vertical wavelength of 21.32 km. In Figure 1, the vertical distance between the stratospheric duct boundaries for the 6.2-min wave is about 37 km (from ~15- to 52-km altitude). Clearly, an integer number of half vertical wavelengths (21.32 km) will not fit in a duct of depth about 37 km and so the 6.2-min wave is not efficiently trapped in the stratospheric duct. A similar analysis (not shown) indicates that the 5.07-min wave does fit well in the stratospheric duct, and so it is efficiently

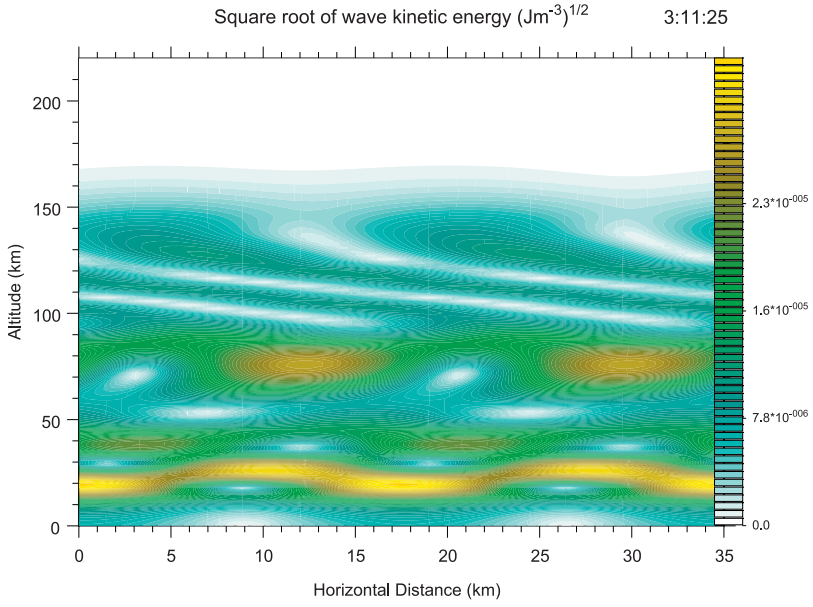

Figure 8. The square root of the wave kinetic energy density, $(u'^2 + w'^2)\rho/2$ of the packet is shown across the spatial grid at a time of about 191 min.

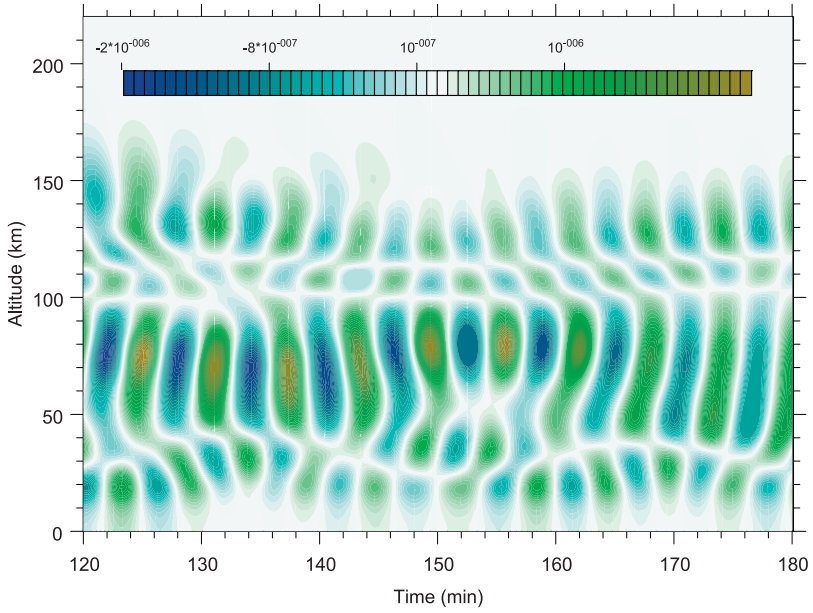

Figure 9. The horizontally averaged wave vertical velocity normalized by the square root of the ratio of the densities $((\rho/\rho_{00})^{1/2}w')$ is shown as a function of altitude and time for the 3rd hour of the simulation.

trapped there. We note that although the 6.2-min wave was not efficiently trapped in the stratospheric duct, it later descended from the mesospheric duct into the stratospheric duct, and eventually it propagated back to the mesospheric duct. The tunneling of this 6.2-min wave through the thin evanescent region near 50-km altitude was seen in the simulations of *Yu and Hickey* [2007]. Similar wave coupling was described by *Fritts and Yuan* [1989], who used the Taylor-Goldstein equation for the vertical velocity and a Wentzel-Kramers-Brillouin (WKB) expression for the vertical wave number to provide a detailed analysis of the ducted wave modes in thermal and Doppler ducts.

[25] Some physical processes have been excluded from our analysis though. One is ion drag that is important for long period gravity waves, but for the high-frequency waves considered here, it will be unimportant [*Hines*, 1968]. *Francis* [1973] also found that the effects of ion drag were nowhere particularly large for the ducted waves that usually are shorter period gravity waves. Furthermore, ion drag usually maximizes at *F*-region altitudes (from about 250- to

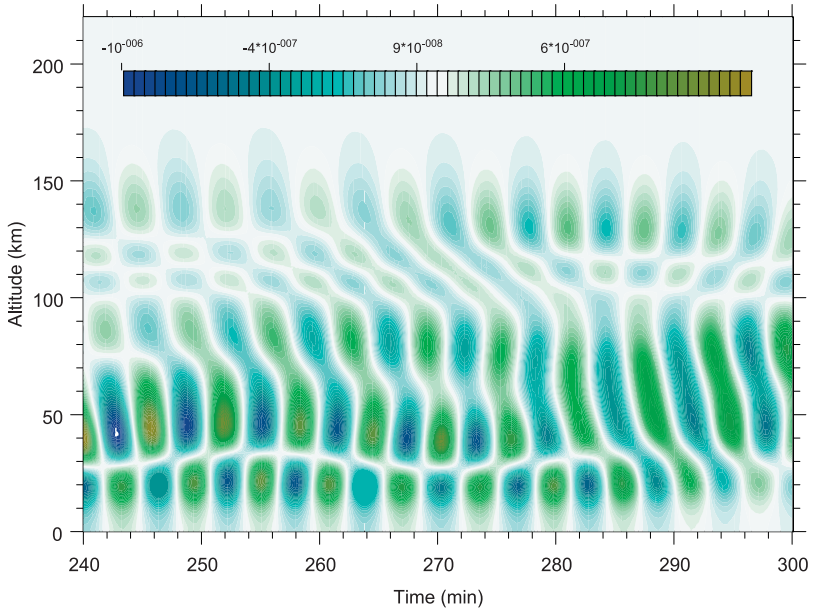

Figure 10. The horizontally averaged wave vertical velocity normalized by the square root of the ratio of the densities $((\rho/\rho_{00})^{1/2}w')$ is shown as a function of altitude and time for the 5th hour of the simulation.

300-km altitude), which are far higher than the altitudes we are interested in here. In addition, for the high-frequency gravity waves ($\omega \gg \Omega_E$, where Ω_E is the angular frequency of the Earth), the effects of the Earth's rotation can be safely neglected [e.g., *Hickey and Cole*, 1987]. Modifications to the dispersion equation including the Coriolis force and ion drag are given by *Volland* [1969], *Francis* [1973], and *Hickey and Cole* [1987].

[26] Because the amplitudes of gravity waves increase with altitude as they propagate upward in a dissipationless atmosphere, they may achieve nonlinear amplitudes and break [e.g., *Fritts*, 1984]. At altitudes below the breaking height, the amplitudes may be large enough to invalidate the dispersion relation (equation (1)) that is based on the linear gravity wave theory. A measure of the importance of nonlinearity is the ratio of the horizontal perturbation velocity to the horizontal phase speed of the wave [e.g., *Fritts*, 1984]. In Figure 4, if we assume that the horizontal perturbation velocity is on an order of the vertical velocity (about 0.8 m/s above 100-km altitude), the horizontal phase speed of the primary wave is about 92.95 m/s, and so the relevant ratio is $\sim$0.01. Because in our study, much of the wave energy resides in high-frequency, fast modes, nonlinear effects in the dispersion relation should never be an issue. Also, *Zhang et al.* [2000] have demonstrated that the dispersion relation based on the linear gravity wave theory is applicable even for the nonlinear cases they considered.

[27] Another process not considered here but which could possibly influence the applicability of equation (1) is the atmospheric baroclinicity [*Jones*, 2005, 2006]. Often the dispersion relation so derived by *Jones* [2005, 2006] ignores acoustic effects by setting the $1/C^2$ terms to zero, but these are important (first order) for the high-frequency waves ($\omega \leq N$) we are studying [*Hickey*, 2001]. In addition, in relation to his equations (29) and (31), *Jones* [2006] has concluded that "For practical purposes, we could probably neglect all of the terms except the first term". This implies that for high-frequency waves, the baroclinicity is, in fact, of lesser importance. We also note that equation (1) applies to an isothermal atmosphere, but nonisothermal effects could only possibly become largest in the lower thermosphere. In any event, we use the dispersion relation to approximately delineate regions of propagation from regions of evanescence, a calculation that is made independent of our numerical model (AGE-TIP). We should also mention that our full-wave and AGE-TIP models do not rely on the use of the WKB approximation. For fast acoustic-gravity waves with large vertical wavelength, dispersion relations like equation (1) that are using the WKB approximation are likely to be suspected [*Einaudi and Hines*, 1971].

[28] The thermosphere is diffusively separated and behaves as a multiconstituent gas where individual species in static equilibrium are each stratified according to their individual scale heights. In contrast, the atmospheric region below the thermosphere is considered well mixed and behaves like a single constituent gas with constant molecular weight up to the turbopause near 105-km altitude. Gravity waves propagating in the thermosphere drive gases out of static equilibrium causing individual gases to oscillate with different amplitudes and phases. Mutual diffusion attempts to mitigate these differences and restore diffusive equilibrium. In the lower thermosphere where mutual diffusion occurs on timescales long compared to typical gravity wave periods, amplitude and phase differences between fluctuating species can be large [*Del Genio et al.*, 1979]. The composition and specific heats of the total gas can be significantly perturbed, and the parcel buoyancy can be significantly affected [*Walterscheid and Hickey*, 2001]. These effects are beyond the scope of our present study, but we note that they may be important for the lower thermospheric ducted modes discussed in this paper.

[29] Because the wave source in our model is a Gaussian function of time, the wave packet generated never reaches a steady state and hence fully ducted modes cannot be achieved. A simulation of fully ducted modes could be possibly performed with the use of a source that reaches constant amplitude for a sufficient length of time to approach a steady state. We have neglected variations that occur in the atmosphere in addition to gravity waves, such as those due to tides and planetary waves [e.g., *Forbes et al.*, 2002]. They are responsible for height-dependent temperature and winds that vary with time. We believe that the basic atmospheric structure can plausibly support ducted wave modes, and the frequent observations of ducted waves that propagate coherently across the field of view of all-sky airglow images [e.g., *Hecht et al.*, 2001] support that belief. They indicate that wave ducting occurs in spite of other variations that are also occurring. Mean winds should also be included in our analysis because our previous full-wave model simulations [*Hecht et al.*, 2001] have shown that winds will modify the ducting process. We plan to examine wind effects on wave ducting using our AGE-TIP model in our future work.

5. Conclusion

[30] Simulations of acoustic-gravity wave propagation in a nonisothermal, dissipative, and initially motionless atmosphere have been performed using a time-dependent, two-dimensional, nonhydrostatic gravity wave model (AGE-TIP). A Gaussian thermal excitation was applied in the troposphere and produced a wave packet that propagated upward. We found that different frequency components of the packet were thermally ducted at different altitudes. A spectral analysis applied at different altitudes successfully identified three wave modes trapped in the stratospheric duct, the MLT duct, and the vertically extended duct lying between the tropopause and the lower thermosphere, respectively. A thin region of evanescence near 90-km altitude partitions the MLT duct into a lower duct (the mesospheric duct) and an upper duct (the lower thermospheric duct).

[31] The periodic coherent QM wave structures that propagated horizontally across airglow images were interpreted by *Hecht et al.* [2001] as gravity waves ducted in the lower thermospheric thermal duct. Our current simulations suggest a possible alternative interpretation wherein the mesospheric duct dominates at airglow altitudes. In that case, the lower thermospheric thermal duct, which is centered near 130-km altitude, would play a secondary role in airglow variations associated with ducted gravity waves. However, we note that waves with different combinations of horizontal wavelength and period may be predominantly ducted in the lower thermospheric thermal duct, and so a

possible ambiguity may exist in the interpretation of some inferences of ducted waves from airglow observations. Note that the lifetime of ducted waves in the mesospheric and lower thermospheric thermal duct certainly suggests that such waves could travel a long distance. By considering the horizontal group velocity of the wave packet at these altitudes, it is quite realistic that the waves could be ducted over a horizontal distance of about 500 km.

[32] Because of the special shape of the thermal structure in the upper and lower atmosphere, a mesospheric plus a lower thermospheric thermal duct, a stratospheric thermal duct, and a vertically extended thermal duct lying between the lower thermosphere and the tropopause (or the ground) must have existed. Some QM waves and only these certain QM waves are determined to be ducted in those regions, even though the propagating wave packet comprises a full spectrum of continuous frequencies. These individual waves will be sorted out and filtered (becoming QM waves) by the thermal structure of the atmosphere. Under certain circumstances, the QM waves containing the resonant frequency (in which their vertical wavelengths satisfy the ducting conditions) could be ducted and trapped in the lower thermospheric thermal duct or other thermal ducts. They could be responsible for the transport of wave-associated energy and momentum over large horizontal distances of several hundreds of kilometers.

[33] **Acknowledgments.** This research was supported by the National Science Foundation under grant ATM-0408407 and by the National Aeronautics and Space Administration under grant NNG04G196G to Embry-Riddle Aeronautical University. We thank the reviewers for their useful comments. We are very grateful to Clia Goodwin for going over our earlier draft carefully and improving its readability.

[34] Amitava Bhattacharjee thanks Douglas ReVelle and another reviewer for their assistance in evaluating this paper.

References

Alexander, M. J. (1996), A simulated spectrum of convectively generated gravity waves: Propagation from the tropopause to the mesopause and effects on the middle atmosphere, *J. Geophys. Res.*, *101*(D1), 1571–1588.

Del Genio, A. D., G. Schubert, and J. M. Straus (1979), Characteristics of acoustic-gravity waves in a diffusively separated atmosphere, *J. Geophys. Res.*, *84*, 1865–1879.

Einaudi, F., and C. O. Hines (1971), WKB approximation in application to acoustic-gravity waves, *Can. J. Phys.*, *48*, 1458–1471.

Forbes, J. M., X. Zhang, W. Ward, and E. R. Talaat (2002), Climatological features of mesosphere and lower thermosphere stationary planetary waves within ±40° latitude, *J. Geophys. Res.*, *107*(D17), 4322, doi:10.1029/2001JD001232.

Francis, S. H. (1973), Acoustic-gravity modes and large-scale traveling ionospheric disturbances of a realistic, dissipative atmosphere, *J. Geophys. Res.*, *78*, 2278–2301.

Friedman, J. P. (1966), Propagation of internal gravity waves in a thermally stratified atmosphere, *J. Geophys. Res.*, *71*, 1033–1054.

Fritts, D. C. (1984), Gravity wave saturation in the middle atmosphere: A review of theory and observations, *Rev. Geophys.*, *22*, 275–308.

Fritts, D. C., and L. Yuan (1989), An analysis of gravity wave ducting in the atmosphere: Eckart's resonances in thermal and Doppler ducts, *J. Geophys. Res.*, *94*(D15), 18,455–18,466.

Hecht, J. H., R. L. Walterscheid, D. C. Fritts, J. R. Isler, D. C. Senft, C. S. Gardner, and S. J. Franke (1997), Wave breaking signatures in OH airglow and sodium densities and temperatures: 1. Airglow imaging, Na lidar, and MF radar observations, *J. Geophys. Res.*, *102*(D6), 6655–6668.

Hecht, J. H., R. L. Walterscheid, M. P. Hickey, and S. J. Franke (2001), Climatology and modeling of quasi-monochromatic atmospheric gravity waves observed over Urbana Illinois, *J. Geophys. Res.*, *106*(D6), 5181–5196.

Hedin, A. E. (1991), Extension of the MSIS thermosphere model into the middle and lower atmosphere, *J. Geophys. Res.*, *96*(A2), 1159–1172.

Hickey, M. P. (1988a), Effects of eddy viscosity and thermal conduction and Coriolis force in the dynamics of gravity wave driven fluctuations in the OH nightglow, *J. Geophys. Res.*, *93*(A5), 4077–4088.

Hickey, M. P. (1988b), Wavelength dependence of eddy dissipation and Coriolis force in the dynamics of gravity wave driven fluctuations in the OH nightglow, *J. Geophys. Res.*, *93*(A5), 4089–4101.

Hickey, M. P. (2001), Airglow variations associated with nonideal ducting of gravity waves in the lower thermosphere region, *J. Geophys. Res.*, *106*(D16), 17,907–17,918.

Hickey, M. P., and K. D. Cole (1987), A quartic dispersion equation for internal gravity waves in the thermosphere, *J. Atmos. Sol. Terr. Phys.*, *49*(9), 889–899.

Hickey, M. P., and Y. Yu (2005), A full-wave investigation of the use of a "cancellation factor" in gravity wave-OH airglow interaction studies, *J. Geophys. Res.*, *110*, A01301, doi:10.1029/2003JA010372.

Hickey, M. P., R. L. Walterscheid, M. J. Taylor, W. Ward, G. Schubert, Q. Zhou, F. Garcia, M. C. Kelly, and G. G. Shepherd (1997), Numerical simulations of gravity waves imaged over Arecibo during the 10-day January 1993 campaign, *J. Geophys. Res.*, *102*(A6), 11,475–11,490.

Hickey, M. P., M. J. Taylor, C. S. Gardner, and C. R. Gibbons (1998), Full-wave modeling of small-scale gravity waves using Airborne Lidar and Observations of the Hawaiian Airglow (ALOHA-93) O (^{1}S) images and coincident Na wind/temperature lidar measurements, *J. Geophys. Res.*, *103*(D6), 6439–6454.

Hickey, M. P., R. L. Walterscheid, and G. Schubert (2000), Gravity wave heating and cooling in Jupiter's thermosphere, *Icarus*, *148*, 266–281.

Hickey, M. P., T.-Y. Huang, and R. L. Walterscheid (2003), Gravity wave packet effects on chemical exothermic heating in the mesopause region, *J. Geophys. Res.*, *108*(A12), 1448, doi:10.1029/2002JA009363.

Hines, C. O. (1960), Internal atmospheric gravity waves at ionospheric heights, *Can. J. Phys.*, *38*, 1441–1481.

Hines, C. O. (1968), An effect of ohmic losses in upper atmospheric gravity waves, *J. Atmos. Sol. Terr. Phys.*, *30*, 851–856.

Hines, C. O., and D. W. Tarasick (1994), Airglow response to vertically standing gravity waves, *Geophys. Res. Lett.*, *21*(24), 2729–2732.

Hocking, W. K. (1987), Turbulence in the region 80–120 km, *Adv. Space Res.*, *7*(10), 171–181.

Isler, J. R., M. J. Taylor, and D. C. Fritts (1997), Observational evidence of wave ducting and evanescence in the mesosphere, *J. Geophys. Res.*, *102*(D22), 26,301–26,313.

Jones, R. M. (2005), A general dispersion relation for internal gravity waves in the atmosphere or ocean, including baroclinicity, vorticity, and rate of strain, *J. Geophys. Res.*, *110*, D22106, doi:10.1029/2004JD005654.

Jones, R. M. (2006), Minimum and maximum propagation frequencies for internal gravity waves, *J. Geophys. Res.*, *111*, D06109, doi:10.1029/2005JD006189.

Pitteway, M. L. V., and C. O. Hines (1965), The reflection and ducting of atmospheric acoustic-gravity waves, *Can. J. Phys.*, *43*, 2222–2243.

Rees, M. H. (1989), Physics and chemistry of the upper atmosphere, Cambridge University Press, Cambridge.

Snively, J. B. (2003), Tropospheric forcing as a source of quasi-monochromatic short-period gravity waves observed in the upper mesosphere and lower thermosphere, MS thesis, Penn State University, University Park.

Snively, J. B., and V. P. Pasko (2003), Breaking of thunderstorm-generated gravity waves as a source of short-period ducted waves at mesopause altitudes, *Geophys. Res. Lett.*, *30*(24), 2254, doi:10.1029/2003GL018436.

Snively, J. B., and V. P. Pasko (2005), Antiphase OH and OI airglow emissions induced by a short-period ducted gravity wave, *Geophys. Res. Lett.*, *32*, L08808, doi:10.1029/2004GL022221.

Strobel, D. F. (1989), Constraints on gravity wave induced diffusion in the middle atmosphere, *Pure Appl. Geophys.*, *130*, 533–546.

Taylor, K. E. (1984), A vertical finite difference scheme for hydrostatic and nonhydrostatic equations, *Mon. Weather Rev.*, *112*, 1398–1402.

Taylor, M. J., M. B. Bishop, and V. Taylor (1995a), All-sky measurements of short period waves imaged in the OI (557.7 nm), Na (589.2 nm) and near infrared OH and O_2 (0, 1) nightglow emissions during the ALOHA-93 campaign, *Geophys. Res. Lett.*, *22*(20), 2833–2836.

Taylor, M. J., Y. Y. Gu, X. Tao, C. S. Gardner, and M. B. Bishop (1995b), An investigation of intrinsic gravity wave signatures using coordinated lidar and nightglow image measurements, *Geophys. Res. Lett.*, *22*(20), 2853–2856.

Volland, H. (1969), The upper atmosphere as a multiple refractive medium for neutral air motions, *J. Atmos. Sol. Terr. Phys.*, *31*, 491–514.

Walterscheid, R. L., and M. P. Hickey (2001), One-gas models with height-dependent mean molecular weight: Effects on gravity wave propagation, *J. Geophys. Res.*, *106*(A12), 28,831–28,840.

Walterscheid, R. L., and G. Schubert (1990), Nonlinear evolution of an upward propagating gravity wave: Overturning, convection, transience and turbulence, *J. Atmos. Sci.*, *47*(1), 101–125.

Walterscheid, R. L., J. H. Hecht, R. A. Vincent, I. M. Reid, J. Woithe, and M. P. Hickey (1999), Analysis and interpretation of airglow and radar observations of quasi-monochromatic gravity waves in the upper mesosphere and lower thermosphere over Adelaide, Australia (35°S, 138°E), *J. Atmos. Sol. Terr. Phys.*, *61*, 461–478.

Walterscheid, R. L., G. Schubert, and D. G. Brinkman (2001), Small-scale gravity waves in the upper mesosphere and lower thermosphere generated by deep tropical convection, *J. Geophys. Res.*, *106*(D23), 31,825–31,832.

Wang, D. Y., and T. F. Tuan (1988), Brunt-Doppler ducting of small period gravity waves, *J. Geophys. Res.*, *93*(A9), 9916–9926.

Yu, Y., and M. P. Hickey (2007), Time-resolved ducting of atmospheric acoustic-gravity waves by analysis of the vertical energy flux, *Geophys. Res. Lett.*, *34*, L02821, doi:10.1029/2006GL028299.

Zhang, S.-D., F. Yi, and J.-F. Wang (2000), The nonlinear effects on the characteristics of gravity wave packets: Dispersion and polarization relations, *Ann. Geophys.*, *18*(10), 1316–1324.

M. P. Hickey and Y. Yu, Department of Physical Sciences, Embry-Riddle Aeronautical University, Daytona Beach, FL 32114, USA. (michael.hickey@erau.edu; yonghui.yu@erau.edu)